



Microstructure, Texture Evolution, and Mechanical Properties of ECAP-Processed ZAT522 Magnesium Alloy

Ying Ma¹ · Fu-Yin Han^{1,2} · Cheng Liu¹ · Ming-Zhe Li¹

Received: 2 July 2019 / Revised: 30 August 2019 / Published online: 2 December 2019
© The Chinese Society for Metals (CSM) and Springer-Verlag GmbH Germany, part of Springer Nature 2019

Abstract

In this work, the high-strength Mg–5Zn–2Al–2Sn (ZAT522, in wt%) Mg alloys was obtained at 220 °C and 130 °C by a two-step equal channel angular pressing (ECAP). For each stage, two passes were used. The results showed a remarkable grain refinement after the first stage of ECAP (A2 samples), leading to a fine-grained structure with average size of 1.40 μm. The additional stage (A4 samples) caused further grain refinement to 1.18 μm, and an ultra-fine grain structure (700 nm) appeared in the precipitate-rich region. The grain refinement mechanism for both samples was discussed in detail. To this end, the original extrusion fiber texture evolved into a new strong texture characterized by the base planes tilted toward the ECAP shear plane, with a higher Schmid factor value of 0.34. Compared with the as-extruded alloy, the yield strength of the A2 samples increased from 180 to 245 MPa, which was mainly attributed to the combined effects of grain boundary strengthening and precipitation strengthening. In the case of A4 samples, the dislocation strengthening resulted in a net increase in yield strength to 335 MPa, while the ductility was significantly reduced.

Keywords Mg–5Zn–2Al–2Sn Mg alloy · ECAP · Microstructure · Texture · Tension properties

1 Introduction

Magnesium wrought alloys with fine grains obtained by dynamic recrystallization (DRX) have better properties and can meet the performance requirements of different applications, such as automobiles and aerospace [1]. At present, commercial wrought Mg alloys are mainly based on Mg–Al series alloys, such as AZ31, AZ80, and AZ91, but they cannot be used at temperatures exceeding 120 °C due to the poor thermal stability of the Mg₁₇Al₁₂ phase [2]. It was reported that the Mg–Zn-based alloys had the greatest potential for application among various Mg alloy systems. Previous studies have proved that Mg–Zn–Al alloys with a Zn/Al weight ratio of about 2:1 or higher have moderate

mechanical properties and good creep resistance [3]. However, their heat resistance and strength cannot completely satisfy the requirements of industrial applications. Further improvement of their properties needs to add rare-earth (RE) elements by alloying techniques [4]. However, owing to the scarcity and high cost of RE elements, low RE and RE-free Mg alloys have become an attracted significant attention in recent years. It was recently discovered that the strength of Mg–Zn–Al alloys can be remarkably enhanced by adding Sn. Adding an appropriate amount of Sn can not only refine the grain size, but also form many high melting point ($T_m = 770$ °C) Mg₂Sn phases, which could prevent hot-cracking during hot working [5]. Wang et al. [6] found that the addition of Sn of 2 wt% yielded the optimal combination of tensile strength and ductility in the as-extruded Mg–4Zn–1.5Al–xSn. The ultimate tensile strength (UTS), yield strength (YS), and elongation (EL) of the alloy were 280 MPa, 147 MPa, and 17.4%, respectively, which is a very promising alloy system. The Mg–5Zn–2Al–2Sn (wt%) (ZAT522) alloy is expected to provide good mechanical properties through subsequent processing and was therefore selected as the target of this study.

When the ultra-fine-grained (UFG) materials with sub-micrometer grain size were obtained by the severe plastic

Available online at <http://link.springer.com/journal/40195>

✉ Fu-Yin Han
hfyty@126.com

¹ School of Materials Science and Engineering, Taiyuan University of Technology, Taiyuan 030024, China

² Shanxi Key Laboratory of Advanced Magnesium-Based Materials, Taiyuan University of Technology, Taiyuan 030024, China

deformation (SPD) technology, such as accumulative roll bonding (ARB) and equal channel angular pressing (ECAP), their mechanical properties can be effectively improved [7–9]. Compared with ARB, by introducing large strains, ECAP has been widely used to prepare bulk UFG metallic materials without changing the shape of the sample. However, the conventional ECAP cannot able to achieve successive processing because the samples need to be manually removed after one pass and reinserted for the next pass, so the number of ECAP passes is usually limited to 10 [10]. At present, as an improved SPD procedure based on ECAP, rotary-die (RD) ECAP can avoid repeated removal and reinsertion of the samples between two successive passes. It can easily used to perform the multi-pass ECAP and has attracted the interest of several researchers in recent years. Liu et al. [11] systematically investigated the $Mg_{97}Y_2Zn_1$ alloy prepared by 16 RD-ECAP passes and found that the ductility had remarkably improved up to 16.5%, which represented an increase by 154% comparing to as-cast alloy.

As is well known, the main slip of wrought Mg alloys at room temperature is basal slip $\{0001\} \langle 11\bar{2}0 \rangle$ because the critical resolved shear stress (CRSS) for non-base slip systems is much larger than that of base slip systems. As the temperature increases, the CRSS of non-base slip decreases gradually, which improves the formability of Mg alloys at elevated temperatures [12]. Therefore, most wrought Mg alloys are currently processed by hot working (> 200 °C). However, due to grain growth and low dislocation density, these wrought Mg alloys do not display the desired performance at elevated temperatures. Thus, many attempts have been made to improve their properties. For example, Kima et al. [13] reported that the grain size of Mg–3Al–1Zn alloy was refined from 5.5 to 1 μm by low-temperature indirect extrusion, and high strength and good ductility were obtained. Thus, deformation of Mg alloys at low temperatures is a feasible method to improve the mechanical properties. Some researchers have attempted to reduce the processing temperature of ECAP [14], or to use extruded alloys as the initial alloy for ECAP processing [15] to prepare Mg alloys with UFG structure. However, researchers have found that low-temperature ECAP processing could introduce different microstructures in wrought Mg alloys, which may result in differing trends in mechanical properties. Yuan et al. [14] obtained a ZK60 Mg alloy with high strength and good ductility by gradually reducing the temperature of ECAP and pre-solution. They reported the UTS and YS of 371 MPa and 260 MPa were obtained by 8 ECAP passes at 150 °C, which was mainly attributed to the grain refinement (500 nm) and more precipitated hierarchically $MgZn_2$ particles. Other studies have reported that low-temperature ECAP does not improve the mechanical properties of Mg alloys. For example, Mostaed et al. [16] obtained an UFG ZM21 Mg alloy with an average size of 0.9 μm through

two-step ECAP at temperatures of 200 °C and 150 °C. They found that the YS did not increase after the second stage of ECAP at 150 °C because the basal planes in most grains were tilted toward the extruded direction (ED), with a higher basal slip Schmid factor value. Moreover, low temperature can reduce the migration rate of atoms, thus delaying the transition of low-angle grain to high-angle grain boundaries and suppressing dynamic recovery [17], which may affect the properties and ductility of Mg wrought alloys. Thus, it is necessary to investigate in-depth on the microstructural characteristics and mechanical properties of Mg alloy processed by ECAP at low temperatures.

In the present work, a high-strength ZAT522 alloy was obtained by low-temperature ECAP in order to improve strength as to change the texture into a new base texture. Two-step ECAP processing with gradually decreasing processing temperature was employed to avoid causing fractures in the samples and improve processing efficiency. Compared to as-cast alloys, as-extruded alloys have better ductility and formability and can yield better microstructure after low-temperature ECAP. Therefore, an as-extruded ZAT522 alloy was used as the initial alloys for low-temperature ECAP processing. The effect of low-temperature ECAP on the microstructural and textural evolution was investigated, in addition to the mechanical behavior of the alloy.

2 Experimental

The studied alloy with the nominal composition Mg–5Zn–2Al–2Sn (wt%) was prepared from high-purity Mg (99.9 wt%), Zn (99.9 wt%), Al (99.99 wt%), and Sn (99.99 wt%) in a crucible resistance furnace. It was protected in a mixed gas of CO_2 and SF_6 (volume ratio = 40:1). Pure Mg was firstly melted at 720 °C. After Mg was completely melted, Zn, Al, and Sn were added. The melt was then refined and maintained at 760 °C for 25 min. Finally, after removing the slag, the melt was poured at 710 °C into a copper mold. An ingot with diameter 75 mm and length 45 mm was homogenized at 350 °C for 40 h, then quenched by cold water, and directly extruded at 300 °C. The extrusion ratio was 16:1, and speed was 0.5 mm/s. The ingot was heated at 300 °C for 30 min before extrusion. After extrusion, the diameter of the extruded bar was 19 mm. The as-extruded samples are designated “A0” hereafter. To fit the die used in ECAP, the ingot samples were first cut into billets of dimensions 12 mm \times 12 mm \times 55 mm. For ECAP, the as-received samples (12 mm \times 12 mm \times 55 mm) were cut into billets from the as-extruded alloy and passed through the adopted ECAP die, which had two cylindrical channels intersecting each other at 110° with an outer arc of curvature 20°. Before ECAP, the temperature of the mold was first raised to the desired value and maintained for 30 min. Subsequently,

a sample coated with a layer of lubricant (graphite powder + petrolatum) was placed in the ECAP mold for 20 min. The extrusion speed was 0.03 mm/s, and the sample was rotated 90° in the same direction between each successive pass (route Bc). The A0 samples were processed by two-step ECAP at decreasing temperatures. As the ZAT522 alloy would have better formability after extrusion, the processing temperature was first decreased to 220 °C for 2 passes of ECAP. The ECAP samples produced in the first stage will be designated as “A2” hereafter. Finally, the temperature was continuously reduced to 130 °C for another 2 passes of ECAP, after which deformation at a lower temperature caused cracking in the samples.

Micrographs were obtained by optical microscopy (OM, DM2700 MRL). The as-extruded and ECAP-processed samples were polished and etched with a mixed solution of 3 g picric acid, 10 mL acetic acid, 50 mL ethanol, and 10 mL distilled water for microstructure observations. Images of the microstructure were acquired by scanning electron microscopy (SEM, Tescan Mira3), and micro-area composition analysis was carried out by energy-dispersive spectroscopy (EDS). The texture of the extruded sample was determined by electron backscatter diffraction (EBSD, Nordlys Nano) with Channel 5 software. The statistical software was Image-Pro Plus 6.0. All samples for observation were obtained from the central part parallel to the extrusion direction.

The tensile testing instrument was used in a WDW-1000 kN electronic testing machine with an initial strain rate of 0.2 mm/min. Tensile specimens with a gauge length of 18 mm, gauge thickness of 2 mm, and gauge width of 4 mm were cut along the ED, and three samples were tested to obtain the average value.

3 Results and Discussion

3.1 Microstructural Characterization

Figure 1 demonstrates the microstructure of the as-received ZAT522 alloys (A0). It can be seen that the extruded samples exhibit a fully dynamically recrystallized microstructure with a bimodal grain size distribution comprising fine and coarse dynamically recrystallized grain. The average grain size was 2.25 μm (Fig. 1b). As seen in Fig. 1c, most of the second phase particles are mainly distributed in the fine grain region along the ED, and the EDS analysis (Fig. 1c) indicates that these particles are Mg₂Sn phase. Due to the particle stimulated nucleation (PSN) mechanism [18], high-stress zones were formed around these particles, which accelerate DRX process and promote grain refinement. In addition, the pinning effect of the fine particles could hinder the growth of the dynamically recrystallized grains in the above regions [19]. As seen in Fig. 1d, the A0 samples

exhibit a strong typical fiber texture with (0001) planes oriented parallel to ED. The maximum intensity of the (0001) basal plane was 8.3.

Figure 2 shows the evolution of the ZAT522 alloys during ECAP and the corresponding SEM images. When the as-extruded ZAT522 alloys were processed by the first stage of ECAP (2 passes at 220 °C, A2 samples), the initial grain size was refined from 2.25 to 1.40 μm with a size distribution from 0.50 to 2.30 μm (Fig. 2a, c). Moreover, after the second stage of ECAP (2 passes at 220 °C in addition to 2 passes at 130 °C, A4 samples), further grain refinement occurred, from 1.40 to 1.18 μm (Fig. 2d, f). This indicates that this two-step ECAP can prevent grain growth with increasing deformation passes at low temperatures. As seen in Fig. 2b, e, the second phase particles still exhibits an inhomogeneous distribution along the extrusion direction, which was consistent with the as-extruded ZAT522 alloys (A0 samples). This precipitate behavior in the low-temperature ECAP processing will be discussed based on the SEM images provided (Fig. 3a–i). Furthermore, the grain boundaries of the A4 samples (Fig. 2e) were blurred, mainly because of the large strain accumulated in grains during low-temperature ECAP.

The SEM images in Fig. 3 show the precipitate-rich (PR) and precipitate-poor (PP) regions during the different deformation stages. Owing to the blurred grain boundary of A4, so we selected a higher-magnification SEM images to observe the microstructure. The detailed microstructural characteristics are summarized in Table 1. As seen in Fig. 3d, g, the A2 and A4 samples still presented a bimodal structure with both coarse and fine grains distributed along the shear direction, mainly related to the distribution of the second phase particles. Moreover, UFG microstructure (0.70 μm) was obtained in the PR region of A4 (Fig. 3h). The influence of ECAP processing temperature will be discussed in the context of precipitate behavior and grain refinement mechanism.

Table 1 lists that the average particle size in A2 and A4 (0.21 μm and 0.17 μm) had decreased compared to that of A0 (0.30 μm), indicating that low-temperature ECAP can effectively refine the grain size of the particles. This is mainly attributed to the dynamic nanometer precipitation and shearing and/or fragmentation of micron-sized particles [20]. Furthermore, the fractions of the second phase particles (16.1% and 17.4%) in A2 and A4 samples were significantly higher than that of A0 (11.2%). The reasons for the increase in this fraction are analyzed in terms of the following two aspects. On the one hand, during the early stage of ECAP, dislocations were first hindered and tangled around the second phase particles. As the number of passes increased, an increasing number of dislocations accumulated around the particles, providing more nucleation sites for the Mg₂Sn phase [21, 22]. On the other hand, with the decrease in the deformation temperature, the dynamic recovery was

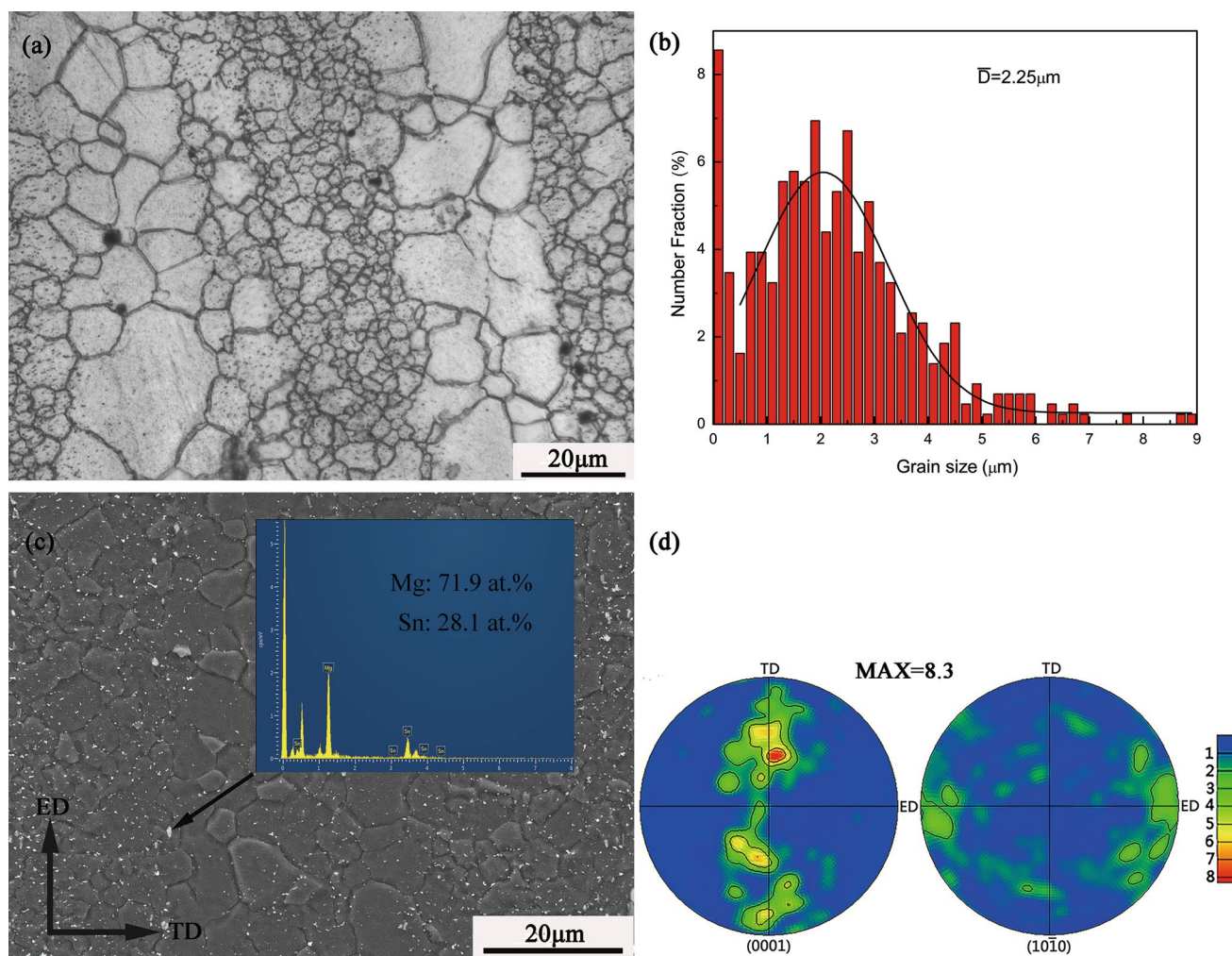


Fig. 1 **a** Microstructure, **b** grain size distribution, **c** SEM micrograph, **d** (0001) and (10-10) pole figures of A0

suppressed, resulting in an increase in the dislocation density, which also promoted the precipitation of the second particles. As mentioned before, in order to obtain a more homogeneous ECAP microstructure in the ZAT522 alloy, hot extrusion was carried out on the investigated samples before ECAP processing. Due to the inhomogeneous distribution of the Sn element in the α -Mg matrix by solution treatment, the second phase particles in the as-extruded alloy showed inhomogeneous distribution (Fig. 3a). However, interestingly, as depicted in Fig. 3d, g, with 2 passes at 220 °C (A2 samples) and 2 additional passes at 130 °C (A4 samples), these particle distribution not only displayed no further homogeneity, but was also still concentrated in the fine grain region. This indicates that the low-temperature ECAP deformation of ZAT522 alloys can only refine the size of the second phase particles, but cannot significantly change its distribution. The reason for this phenomenon may be related to the particles distribution of the as-extruded alloys, which may also be related to the composition of the

phase [23], and detailed analyses are currently being conducted. As we know, the pinning effect of the fine particles could hinder the growth of the dynamically recrystallized grains [24]. Therefore, the inhomogeneous distribution of these fine particles plays an important role in restricting grain growth, resulting in the grain size of PR region significantly smaller than that of PP region in A2 and A4 samples.

Another influence of ECAP processing temperature on the microstructure was the grain refinement mechanisms. The recrystallized fractions of ECAP-processed alloys are evaluated from the EBSD patterns with different types of grains. The results are shown in Fig. 4, in which blue indicates recrystallized grains, yellow indicates substructures (dislocations and sub-boundaries), and red indicates highly deformed grains. It can be seen that A2 samples exhibit a higher fractions of recrystallized grains and some substructured grains which mainly consist of relatively coarse grains. The fractions of recrystallized and substructured grains in the A2 sample are 70.4%, 28.9%, respectively. However,

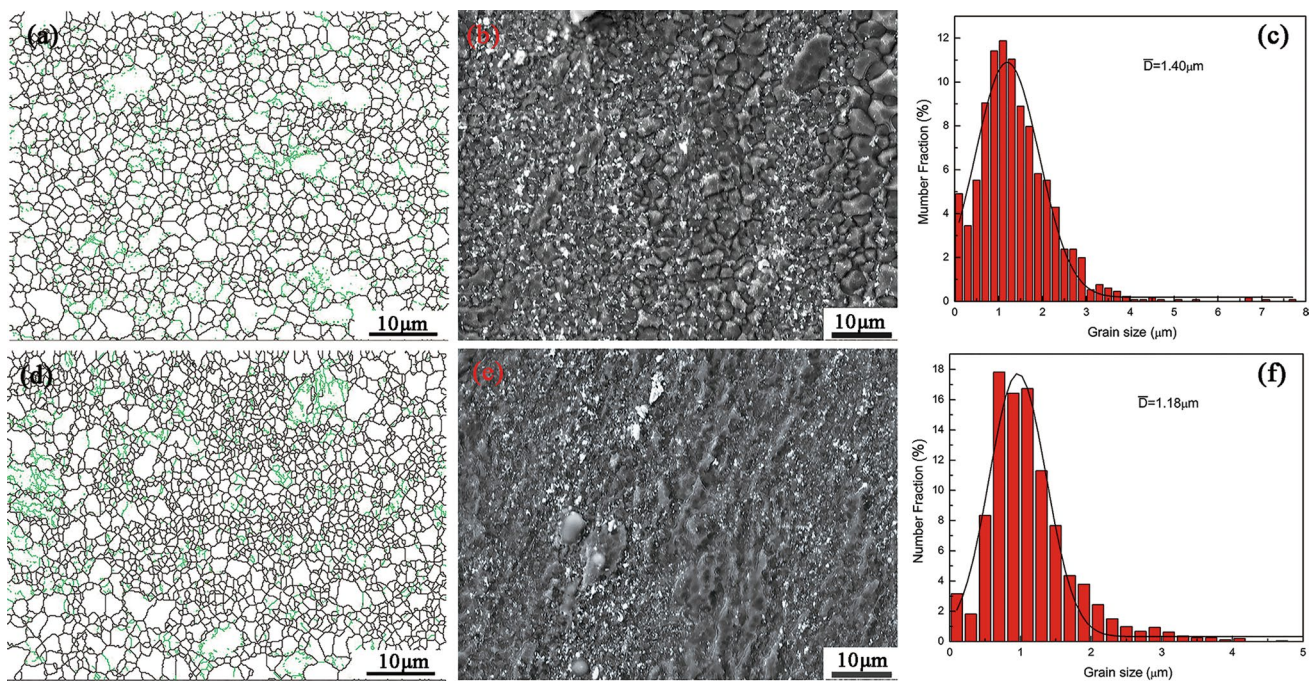


Fig. 2 Grain boundary map **a, d**, SEM micrographs **b, e** and grain size distributions **c, f** of the ECAP samples: **a–c** A2, **d–f** A4

after second stage of ECAP, a significant decrease in the recrystallization tendency was observed in A4 samples, while the fraction of the substructured grains was remarkably increased, including both coarse and fine grains. The fractions of recrystallized and substructured grains in the A4 sample are 42.4% and 54.7%, respectively. These results show that the microstructure evolution of low-temperature ECAP is closely related to the processing temperature. As the processing temperature was gradually reduced, the dynamic recovery in the alloy was suppressed, resulting in an increase in dislocation density and subgrain boundaries. These dislocations form subgrain boundaries and divide the original grains into small subgrains, further refining the grains [25]. It should be noted that the relatively small ($< 1 \mu\text{m}$) second phase particles in the ECAP-processed samples indicate a relatively weak PSN effect and also cause a decrease in the recrystallization fraction [18, 26], especially in the PP region with few secondary particles. Therefore, it could be concluded that the refinement mechanism of the A2 samples is mainly recrystallization refinement, and substructure refinement occurs in the coarse grain region. With increasing the ECAP passes, a large amount of subgrains were introduced into the A4 samples, which was attributed to the further decreasing dynamic recovery rate and the weak PSN effect. Thus, the refinement mechanism of A4 samples is mainly subgrain refinement. In other words, the formation of a large number of subgrains is the main reason of grain size reduction, overwhelming the refinement effect of dynamic recrystallization.

3.2 Texture Evolution

The (0002) pole figures of A2 and A4 processed by ECAP are shown in Fig. 5. After the first stage of ECAP, the texture of the base plane parallel to the ED in the A0 samples weakens; however, the strongest component of the base plane remains in A2. Therefore, the texture of A2 was similar to the fiber texture of A0, with a reduced maximum texture strength from 8.30 to 7.41. As the A2 samples undergo the second stage of ECAP, a new texture formed along the shear plane in A4 samples completely replaced the original fiber texture, and the strongest pole in the base texture was approximately 30° from the ED. Its maximum texture intensity increases from 7.41 to 8.98. The same texture evolution could also be observed in ECAP-processed ZK60 Mg alloy [27]. Such evolution of the texture formed by ECAP is mainly due to a highly redundant stress accumulated along the route Bc [28].

The Schmid factor (SF) distribution for (0 0 0 1) $\langle 1\ 1\ 2\ 0 \rangle$ base plane of the investigated samples (Fig. 6) reveals that with increasing the ECAP passes, the value of SF gradually increases, from 0.21 (A0) to 0.25 and 0.34 for A2 and A4 samples, respectively. It should be noted that at room and moderate elevation temperature, the plastic deformation of Mg alloys is mainly governed by the slip of the base plane [12]. Thus, the SF value for base slip systems plays a key role in the mechanical properties of Mg alloys. When the base plane in the A4 samples was rotated 30° toward to ED, the SF value of the base slip was significantly higher

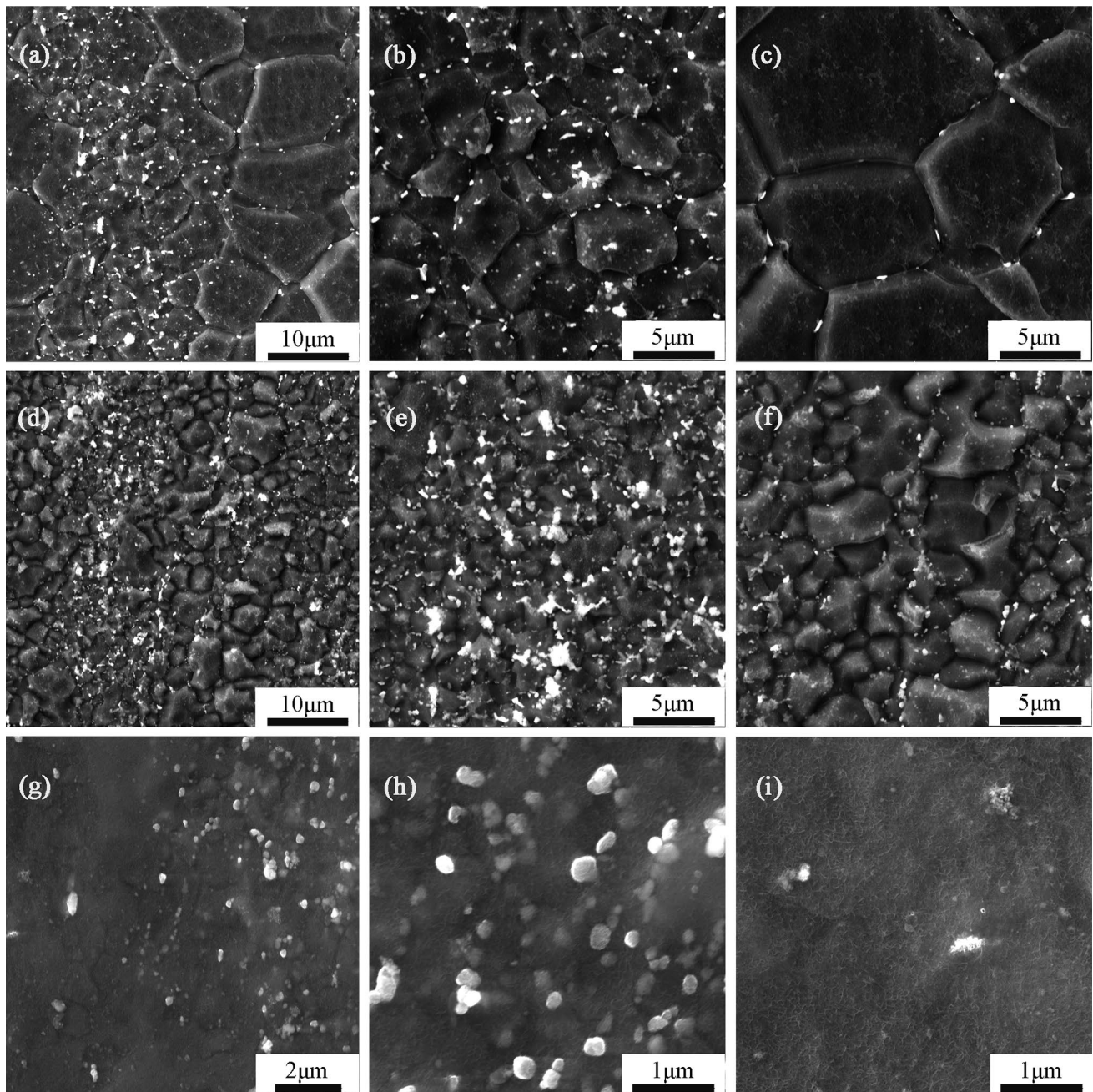


Fig. 3 SEM micrographs showing **a, d, g** both precipitate-rich (PR) and precipitate-poor (PP) regions, **b, e, h** only RP region, and **c, f, i** only PP region of the as-extruded A0 **a–c**, the ECAP-processed **d–f** A2, **g–i** A4 samples

at 0.34 (Fig. 6c) which was consistent with the evolution of the texture. This easily made the dislocation slip on the main sliding plane (0 0 0 1), reducing the stress required for yield.

3.3 Mechanical Properties

Figure 7 shows the stress–strain curves of the as-received and ECAP-processed samples. Data for TYS, UTS, and EL are summarized in Table 1. It can be seen that YS increased

from 180 to 245 MPa due to significant grain refinement from A0 (2.25 μm) to A2 (1.40 μm) samples. However, no marked change in tensile strength was observed. At the same time, there was a slight decrease in elongation. It should be noted that an increase in strength was observed, although the weakening of the initial fiber texture and high Schmid factor was detected in A4 samples. In addition, compared with the as-received condition (A0 samples), the volume fraction of fine second phase particles in A2 sample increased

Table 1 Microstructure characteristics of the ECAP ZAT522 samples

State	Microstructure					Mechanical properties		
	d_{avg} (μm)	d_{PR} (μm)	d_{PP} (μm)	d_{p} (μm)	f_{p} (%)	YS (MPa)	UTS (MPa)	EL (%)
A0	2.25 ± 0.02	5.65 ± 0.04	2.04 ± 0.06	0.27 ± 0.05	11.2 ± 0.4	180 ± 3	320 ± 4	33.4 ± 0.03
A2	1.40 ± 0.04	1.20 ± 0.02	1.91 ± 0.05	0.21 ± 0.04	16.1 ± 0.2	245 ± 2	325 ± 3	26.2 ± 0.02
A4	1.18 ± 0.02	0.70 ± 0.05	1.39 ± 0.03	0.17 ± 0.02	17.4 ± 0.5	335 ± 2	356 ± 3	10.7 ± 0.03

d_{avg} presents the average grain size of the ECAP-processed samples. d_{PR} and d_{PP} present the average grain size of precipitate-rich (PR) and precipitate-poor (PP) regions, respectively. d_{p} and f_{p} represent the volume fraction and average grain size of precipitates, respectively. YS, UTS, and EL represent tensile yield strength, ultimate tensile strength, and elongation

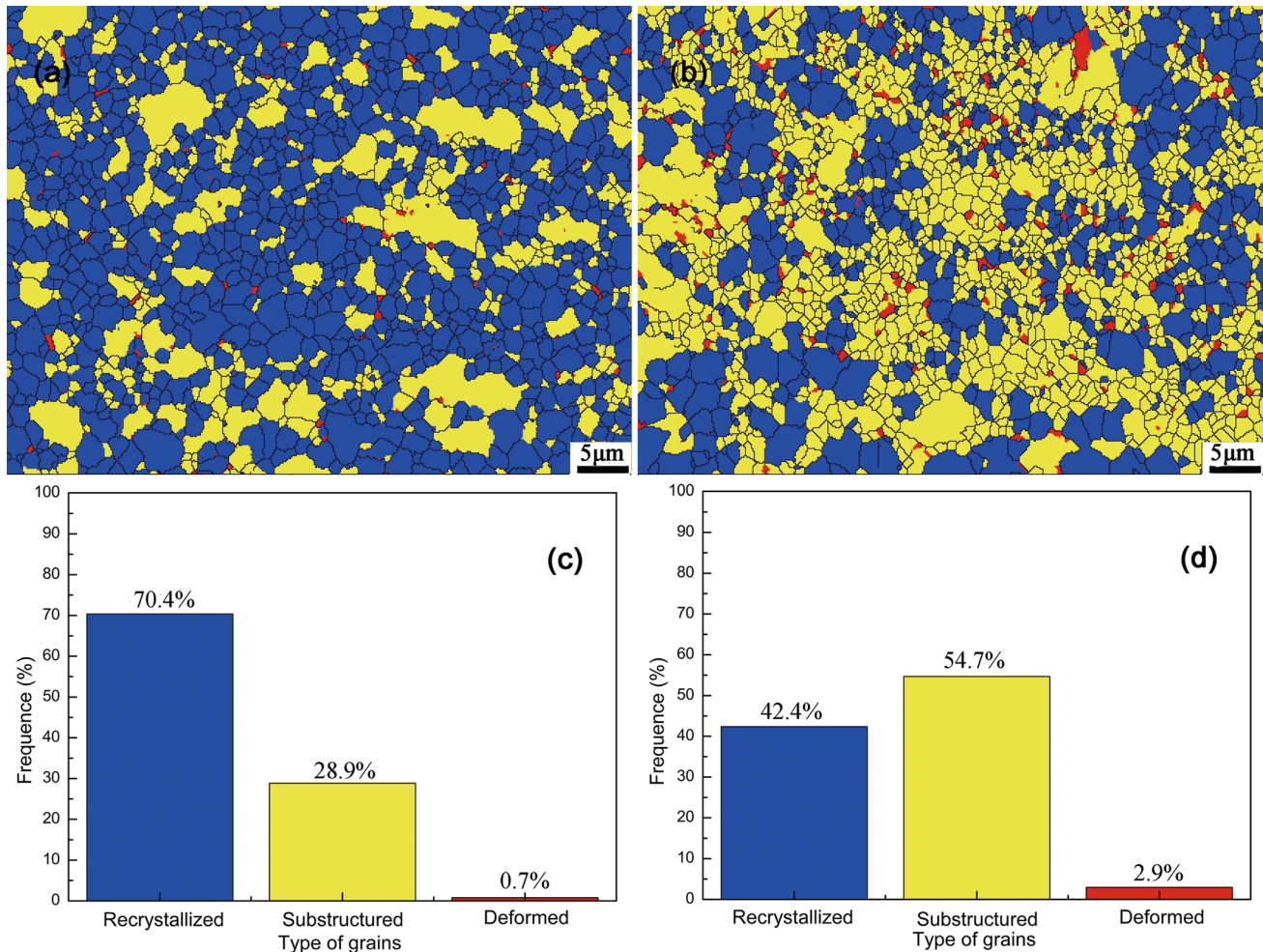


Fig. 4 Different types of grains of the ECAP-processed ZAT522 alloys **a** A2, **b** A4: blue-recrystallized, yellow-substructured, red-deformed; **c** and **d** frequency of the different types of grains as shown in **a**, **d**, respectively

from 11.2% to 16.1%. These fine particles can effectively hinder dislocation movement and grain boundary migration during tension, leading to the dispersion strengthening effect on the A2 sample. Therefore, it can be stated that the main mechanism for A2 samples was grain boundary and dispersion strengthening, resulting in a net increase in YS. In the case of A4 samples, both YS and UTS significantly

increased from 245 and 325 MPa up to 335 and 356 MPa, respectively. However, interestingly, the EL decreased from approximately 26.2–10.7%. As discussed before, resulted in a newly formed shear texture in the A4 sample (Fig. 5b), by which the base plane in most grains was inclined at an angle of about 30° to the ED with the highest basal slip and SF value (0.34), resulting to the required YS in the plastic

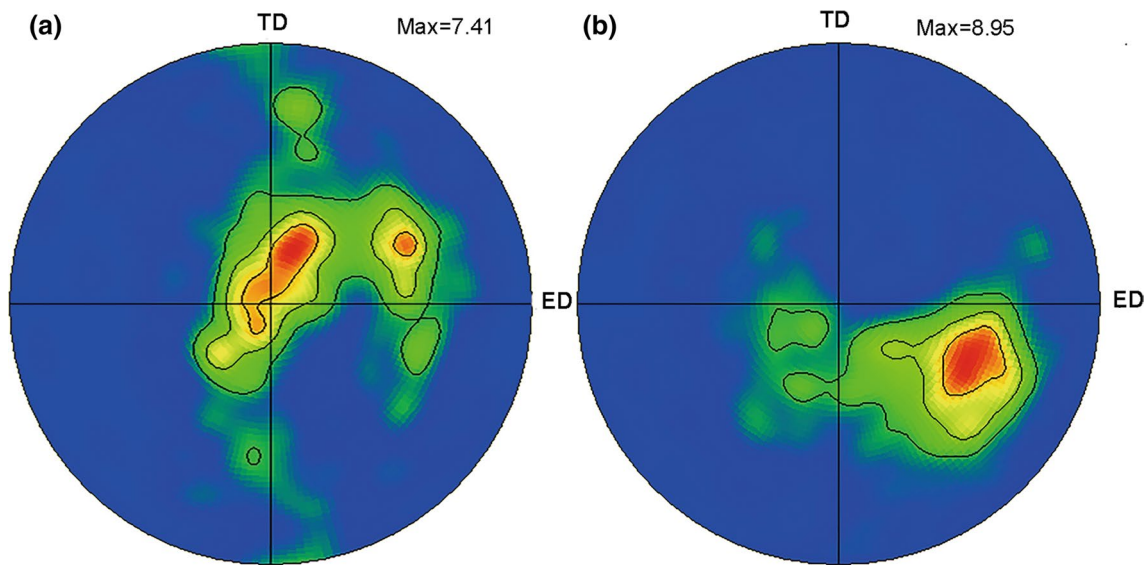


Fig. 5 (0002) pole figures of the ECAP-processed ZAT522 alloys: **a** A2, **b** A4

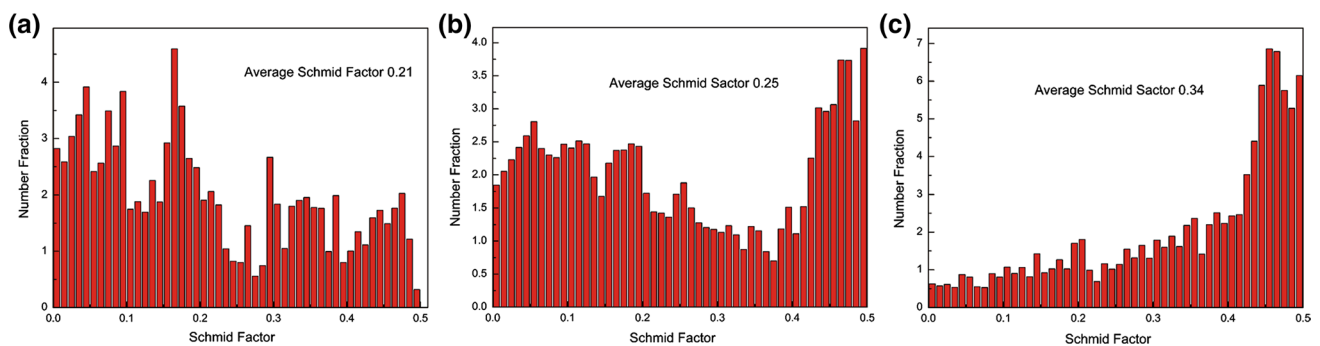


Fig. 6 Distributions of Schmid factors for the (0001) $\langle 10\text{-}20 \rangle$ base slip of the deformed samples: **a** A0, **b** A2, **c** A4

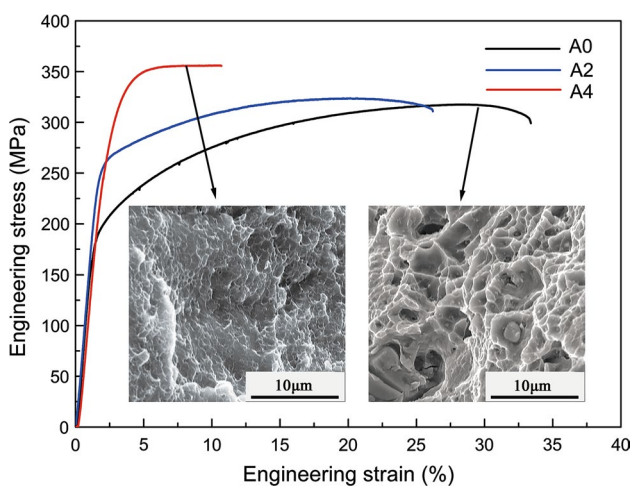


Fig. 7 Tensile stress–strain curves of the deformed ZAT522 alloys, and corresponding SEM views of the fracture surfaces of A2 and A4 samples

deformation was reduced. The above analysis of the microstructure evolution of the ECAP-processed alloy shown that the dynamic recrystallization fraction decreases in the A4 samples, and the dislocation density increases sharply, resulting in a significant dislocation strengthening effect. In addition, the grain refinement effect of the A4 sample was not as good as that of the A2 sample, and the second phase fraction and size did not change much. Therefore, it could be concluded that dislocation enhancement is a dominating factor in the A4 samples, overwhelming the weakening effect of the texture and resulting in a net increase in YS and UTS.

A significant drop in elongation of the A4 samples can be explained by microstructural features. First, in the fine-grained polycrystalline Mg alloy, there is enhanced activation of non-basal slip systems at room temperature due to grain boundary compatibility stress and grain boundary sliding [29]. Hence, the shear texture formed in the ECAP-processed alloy as well as the greater texture strength and

SF value result in easier basal slip during tensile testing [30]. Both of the above aspects are beneficial to improve the ductility of the A4 samples. However, as stated, the most striking feature of the A4 sample was the large number of dislocations accumulated in the grains at low-temperature ECAP. The accumulation of these high-density dislocations caused severe strain concentrations, resulting in a significant decrease in the elongation of the A4 sample. In addition, the difference between UTS and YS can be used to define the work-hardening ability ($H_c = (UTS - YS)/YS$) [31], which strongly supports the effective assumption that the effect of strain concentration in tensile test. According to the formula and the mechanical properties of the investigated alloys in Table 1, the work-hardening abilities of the A0, A2, and A4 samples are 0.78, 0.33, and 0.06, respectively. The lowest HC value in the A4 sample indicates a higher sensitivity to stress concentration, which is not conducive to enhancement in ductility. In short, the combined effect of grains, texture evolution, and H_c value resulted in a significant decrease in the EL of the A4 sample.

Figure 7 represents SEM fractographs of samples A0 and A4. Dense and finer dimples can be distinctly seen in SEM fractographs for A0 samples, suggesting dislocation slips were more active and can improve ductility of the A0 samples [32]. Furthermore, some secondary phases were observed in the dimples, and some microcracks could be seen on these particles. It is suggested that the cleavage of secondary phase particles is the main reason for failed ductility. In contrast, the smaller dimples were also apparent for the A4 samples, but their dimensions were much smaller than those found under the A0 condition due to the marked refinement of the grains. However, the dimple depth of the A4 became shallower, which means that its plastic deformation ability was relatively poor. This is mainly attributed to the stress accumulated in grains. Thus, it can be concluded that the failure ductility of the A4 samples has occurred before fully entering the plastic deformation stage during the tensile test, which was consistent with the trend of the stress–strain curve in Fig. 7.

4 Conclusions

The microstructure and tensile properties of low-temperature ECAP-processed alloys have been investigated. The main conclusions were summarized as follows:

1. After several ECAP passes (i.e., 2 passes at 220 °C in addition to 2 passes at 130 °C), significant grain refinement was obtained with an average size of 1.18 μm , and an ultra-fine grain structure (700 nm) appeared in the precipitate-rich region. The ECAP-processed alloy showed finer grain size of the second particles, and they were still mainly distributed in relatively fine grain region.
2. The texture evolution of the as-received ZAT522 alloy in ECAP processed was studied in detail. The initial fiber texture of the ZAT522 extruded alloy gradually decomposed during two-step ECAP at decreasing temperatures. After 4 passes, a new texture type formed in A4 at 30° to the ED, which completely replaced the original fiber texture, with a higher basal slip texture and Schmid factor value of 0.34.
3. Significant grain refinement and dispersion strengthening resulted in a notable increase in the YS of the A2 samples from 180 to 245 MPa, without much loss in ductility. As deformation proceeded, the dislocation strengthening resulted in a net increase in YS of the A4 sample to 335 MPa, while higher dislocations resulted in a poor ductility.

Acknowledgements This study was supported by the National Natural Science Foundation of China (Grant Nos. 51874209 and 51771129).

References

- [1] Z. Yang, J.P. Li, J.X. Zhang, G.W. Lorimer, J. Robson, *Acta Metall. Sin. (Engl. Lett.)* **21**, 328 (2008)
- [2] J. Bai, Y.S. Sun, S. Xun, F. Xue, T.B. Zhu, *Mater. Sci. Eng. A* **419**, 1 (2006)
- [3] Y. Zhang, X.F. Huang, Z.D. Ma, Y. Li, F. Guo, J.C. Yang, Y. Ma, Y. Hao, *Mater. Sci. Eng. A* **686**, 93 (2017)
- [4] S.J. Meng, H. Yu, S.D. Fan, Q.Z. Li, S.H. Park, J.S. Suh, Y.M. Kim, X.L. Nan, M.Z. Bian, F.X. Yin, W.M. Zhao, B.S. You, K.S. Shin, *Acta Metall. Sin. (Engl. Lett.)* **32**, 145 (2019)
- [5] P. Cao, M.L. Zhang, W. Han, Y.D. Yan, L.J. Chen, *Acta Metall. Sin. (Engl. Lett.)* **25**, 265 (2012)
- [6] B. Wang, X.H. Chen, F.S. Pan, J.J. Mao, *Prog. Nat. Sci.* **27**, 695 (2017)
- [7] Y. Wang, H.J. Wu, X.T. Liu, Y.L. Jiao, J.F. Sun, R.Z. Wu, L.G. Hou, J.H. Zhang, X.L. Li, M.L. Zhang, *Mater. Sci. Eng. A* **761**, 138049 (2019)
- [8] H.J. Wu, T.Z. Wang, R.Z. Wu, L.G. Hou, J.H. Zhang, X.L. Li, M.L. Zhang, *J. Mater. Process. Tech.* **254**, 265 (2018)
- [9] L.G. Hou, T.Z. Wang, R.Z. Wu, J.H. Zhang, M.L. Zhang, A.P. Dong, B.D. Sun, S. Betsofen, B. Krit, *J. Mater. Sci. Technol.* **34**, 317 (2018)
- [10] H. Liu, H. Huang, C. Wang, J.P. Sun, J. Bai, F. Xue, A.B. Ma, X.B. Cheng, Recent advances in LPSO-containing wrought magnesium alloys: relationships between processing, microstructure, and mechanical properties. *JOM* (2019). <https://doi.org/10.1007/s11837-019-03610-9>
- [11] H. Liu, J. Ju, X.W. Yang, J.L. Yan, D. Song, J.H. Jiang, A.B. Ma, *J. Alloys Compd.* **704**, 509 (2017)
- [12] B. Srinivasarao, N.V. Dudamel, M.T. Pérez-Prado, *Mater. Charact.* **75**, 101 (2013)
- [13] B. Kima, C.H. Park, H.S. Kim, B.S. You, S.S. Park, *Scr. Mater.* **76**, 21 (2014)
- [14] Y.C. Yuan, A.B. Ma, X.F. Gou, J.H. Jiang, G. Arhin, D. Song, H. Liu, *Mater. Sci. Eng. A* **677**, 216 (2016)

- [15] M. Gzyl, A. Rosochowski, S. Boczkal, L. Olejnik, *Mater. Sci. Eng. A* **638**, 20 (2015)
- [16] E. Mostaed, A. Fabrizi, D. Dellasega, F. Bonollo, M. Vedani, *J. Alloys Compd.* **638**, 267 (2015)
- [17] D.H. Shin, J.J. Pak, Y.K. Kim, K.T. Park, Y.S. Kim, *Mater. Sci. Eng. A* **323**, 409 (2002)
- [18] K. Huang, R.E. Logé, *Mater. Des.* **111**, 548 (2016)
- [19] K. Sheng, L.W. Lu, Y. Xiang, M. Ma, Z.C. Wang, *Acta Metall. Sin. (Engl. Lett.)* **32**, 235 (2019)
- [20] W.L. Cheng, L. Tian, S.C. Ma, Y. Bai, H.X. Wang, *Materials* **10**, 708 (2017)
- [21] F.-D. Dumitru, O.F. Higuera-Cobos, J.M. Cabrera, *Mater. Sci. Eng. A* **594**, 32 (2014)
- [22] R. Jahadi, M. Sedighi, H. Jahed, *Mater. Sci. Eng. A* **593**, 178 (2014)
- [23] T. Liu, W. Zhang, S.D. Wu, C.B. Jiang, S.X. Li, Y.B. Xu, *Mater. Sci. Eng. A* **360**, 345 (2003)
- [24] Y. Bai, W.L. Cheng, S.C. Ma, J. Zhang, C. Guo, Y. Zhang, *Acta Metall. Sin. (Engl. Lett.)* **31**, 41 (2018)
- [25] Y.B. He, Q.L. Pan, Y.J. Qin, X.Y. Liu, W.B. Li, Y.L. Chiu, J. Chen, *Chin. J. Nonferr. Metal.* **20**, 2274 (2010)
- [26] C.J. Wang, K.K. Deng, S.S. Zhou, W. Liang, *Acta Metall. Sin. (Engl. Lett.)* **29**, 527 (2016)
- [27] E. Mostaed, M. Hashempour, A. Fabrizi, D. Dellasega, M. Bestetti, F. Bonollo, M. Vedani, *J. Mech. Behav. Biomed.* **37**, 307 (2014)
- [28] A. Gholinia, P.B. Prangnell, M.V. Markushev, *Acta Mater.* **48**, 1115 (2000)
- [29] J. Koike, T. Kobayashi, T. Mukai, H. Watanabe, M. Suzuki, K. Maruyama, K. Higash, *Acta Mater.* **51**, 2055 (2003)
- [30] P. Yang, L.N. Wang, X. Li, L. Meng, *Acta Metall. Sin. (Engl. Lett.)* **23**, 63 (2010)
- [31] N. Afrin, D.L. Chen, X. Cao, M. Jahazi, *Scr. Mater.* **57**, 1004 (2007)
- [32] J.L. Wang, Y.C. Guo, J.L. Li, Z. Yang, S. Kamado, L.M. Wang, *J. Alloys Compd.* **653**, 100 (2015)